Driving Mechanisms of an Extreme Winter Sea Ice Breakup Event in the Beaufort Sea

Jonathan W Rheinlænder, Richard Davy, Einar Ólason, Pierre Rampal, Clemens Spensberger, Timothy D Williams, Anton Korosov, Thomas Spengler

Geophysical Research Letters

RESEARCH LETTER
10.1029/2022GL099024

Driving Mechanisms of an Extreme Winter Sea Ice Breakup Event in the Beaufort Sea

Jonathan W. Rheinlænder[1,2], Richard Davy[1], Einar Ólason[1], Pierre Rampal[3], Clemens Spensberger[4], Timothy D. Williams[1], Anton Korosov[1], and Thomas Spengler[4]

[1]Nansen Environmental and Remote Sensing Center and Bjerknes Centre for Climate Research, Bergen, Norway, [2]Department of Earth Science, University of Bergen, and Bjerknes Centre for Climate Research, Bergen, Norway, [3]Institut de Géophysique de l'Environnement, Université Grenoble Alpes/CNRS/IRD/G-INP, Grenoble, France, [4]Geophysical Institute, University of Bergen, and Bjerknes Centre for Climate Research, Bergen, Norway

Key Points:

- An extreme winter breakup event in the Beaufort Sea is accurately simulated with the neXtSIM sea ice model
- High-resolution and skillful atmospheric forcing, as well as appropriate sea ice rheology, are necessary to simulate such breakups
- In the model, thinning Beaufort Sea ice is more vulnerable to breakup, which may accelerate loss of multiyear ice

Supporting Information:

Supporting Information may be found in the online version of this article.

Correspondence to:

J. W. Rheinlænder,
jonathan.rheinlaender@nersc.no

Citation:

Rheinlænder, J. W., Davy, R., Ólason, E., Rampal, P., Spensberger, C., Williams, T. D., et al. (2022). Driving mechanisms of an extreme winter sea ice breakup event in the Beaufort Sea. *Geophysical Research Letters*, *49*, e2022GL099024. https://doi.org/10.1029/2022GL099024

Received 4 APR 2022
Accepted 9 JUN 2022

Author Contributions:

Conceptualization: Jonathan W. Rheinlænder, Richard Davy, Pierre Rampal, Thomas Spengler
Data curation: Jonathan W. Rheinlænder, Clemens Spensberger, Timothy D. Williams
Formal analysis: Jonathan W. Rheinlænder, Anton Korosov
Funding acquisition: Richard Davy, Einar Ólason
Investigation: Jonathan W. Rheinlænder
Project Administration: Richard Davy, Einar Ólason
Resources: Clemens Spensberger, Timothy D. Williams, Anton Korosov

Abstract The thick multiyear sea ice that once covered large parts of the Arctic is increasingly being replaced by thinner and weaker first-year ice, making it more vulnerable to breakup by winds. We use the neXtSIM sea ice model to investigate the driving mechanisms behind a large breakup event in the Beaufort Sea during winter 2013. Our simulations are the first to successfully reproduce the timing, location, and propagation of sea ice leads associated with wind-driven breakup and highlight the importance of accuracy of the atmospheric forcing, sea ice rheology, and changes in sea ice thickness. We found that the breakup resulted in enhanced export of multiyear ice from the Beaufort Sea. Overall, this leads to a relatively thinner and weaker simulated ice cover that potentially preconditions earlier breakup in spring and accelerates sea ice loss. Finally, our simulations indicate that large breakup events could become more frequent as Arctic sea ice continues to thin.

Plain Language Summary The loss of thick multiyear sea ice in the Arctic leads to weaker sea ice that is more easily broken up by strong winds. As a consequence, extreme sea ice breakup events may become more frequent, even during the middle of winter when the sea ice cover is frozen solid. This can lead to an earlier onset of the melt season and potentially accelerate Arctic sea ice loss. Such extreme breakup events are generally not captured by climate models, potentially limiting our confidence in projections of Arctic sea ice. We investigated the driving forces behind sea ice breakup events during winter and how they change in a future climate. Our sea ice model is the first to reproduce such breakup events and reveals that the combination of strong winds and thin sea ice is a key factor for these breakups. We found that winter breakups have a large effect on local heat and moisture transfer and cause enhanced sea ice production, but also increase the overall movement of the sea ice cover, making it more vulnerable. Finally, we show that if the Arctic sea ice continues to thin, these extreme breakup events could become even more frequent.

1. Introduction

Arctic sea ice is thinning (Meier, 2017) in conjunction with the decrease in the area covered by thick multiyear ice (MYI) (Kwok, 2018), which is replaced by thinner first-year ice (FYI) that is more mobile and less dynamically stable (Rampal et al., 2009; J. Zhang et al., 2012). This makes the ice cover more vulnerable to intense winds breaking up the sea ice. In the Beaufort Sea in particular, the loss of MYI may contribute to the earlier onset of the melt season in recent years (Johnson & Eicken, 2016).

When sea ice breaks up, it exposes the underlying warmer ocean within narrow, linear openings in the ice cover known as leads. This has important consequences for air-sea exchange, ocean eddy generation and dynamics, sea ice production, and Arctic Ocean properties in general (Cohanim et al., 2021; Graham et al., 2019; Nguyen et al., 2009), especially during the winter months when heat fluxes over sea ice are generally small (Andreas & Cash, 1999). In addition, breakup in winter weakens the ice cover, potentially preconditioning the minimum ice extent in summer (Y. Zhang et al., 2018; Babb et al., 2019) and thus creating a positive feedback to Arctic amplification (Dai et al., 2019). Therefore, extreme breakup events are of crucial interest for understanding the seasonal and long-term evolution of Arctic sea ice, which in turn affect weather, ecosystems, and local communities in polar regions and beyond (Forbes et al., 2016; Vihma, 2014).

Supervision: Richard Davy, Einar Ólason
Validation: Jonathan W. Rheinlænder, Timothy D. Williams, Anton Korosov
Visualization: Jonathan W. Rheinlænder
Writing – original draft: Jonathan W. Rheinlænder, Richard Davy, Einar Ólason, Pierre Rampal, Timothy D. Williams
Writing – review & editing: Jonathan W. Rheinlænder, Einar Ólason, Pierre Rampal, Clemens Spensberger, Thomas Spengler

Several studies have investigated the impact of storms on Arctic sea ice cover (e.g., J. Zhang et al., 2013; Graham et al., 2019; Wang et al., 2016). However, when it comes to modeling individual breakup events, and accurately reproducing the spatial distribution of leads, there have been few successful attempts (Ólason, Rampal, & Dansereau, 2021; Wang et al., 2016), and breakup events are not well captured in current sea ice and climate models (Spreen et al., 2017). This presents a critical gap in our understanding of atmosphere-ocean-ice interaction processes and limits the credibility of future projections of the climate in polar and subpolar regions (Notz & Stroeve, 2016).

This paper is the first step toward filling this gap by presenting simulations using the next-generation sea ice model—neXtSIM (Ólason, Rampal, & Dansereau, 2021; Rampal et al., 2016, 2019; Samaké et al., 2017)—focusing on a large breakup event that occurred in the Beaufort Sea during February and March 2013. This event was captured by the Visible Infrared Imaging Radiometer Suite of the Suomi NPP satellite (Beitsch et al., 2014) and coincided with a high-pressure system centered over the northwest Beaufort Sea (Figure 1a). The objective of this study is to identify the key factors driving such wintertime sea ice breakup events, and provide a first estimate of the consequences of these events for the Arctic sea ice volume budget.

2. neXtSIM Model Setup

All simulations presented here are performed with the stand-alone version of neXtSIM, which is a finite element sea ice model using a moving Lagrangian mesh (Bouillon & Rampal, 2015; Rampal et al., 2016). The spatial resolution of the mesh is about 10 km, covering the central Arctic. Sea ice mechanics are reproduced using the Brittle Bingham-Maxwell (BBM) rheology based on a damage propagation mechanism (Dansereau et al., 2016; Girard et al., 2011; Ólason, Boutin, et al., 2021). This allows for realistic reproduction of cracks and leads in the ice cover (Ólason, Rampal, & Dansereau, 2021; Rampal et al., 2019), making the neXtSIM ideal for simulating breakup events. Other relevant model settings are listed in Table S1 of Supporting Information S1.

The model is forced by hourly atmospheric fields from the polar-optimized version of the Weather Research and Forecasting (WRF) model version 3.9.1 (Polar-WRF; Hines et al., 2015; Powers et al., 2012). The WRF output is a dynamical downscaling of the European Centre for Medium Range Weather Forecasts (ECMWF) operational analysis with interior nudging toward the ECMWF analysis. We tested four different horizontal resolutions (10, 20, 40, and 80 km) to investigate the role of atmospheric resolution on simulating the 2013 breakup event. These are referred to as WRF10, WRF20, WRF40, and WRF80. To test the impact of not using a polar-specific atmospheric model, we also used the standard global reanalysis from ERA5 (Hersbach et al., 2020) with a horizontal resolution of 31 km (Figure S2 in Supporting Information S1). All neXtSIM simulations are initialized with sea ice fields from CS2/SMOS (Ricker et al., 2017) and are integrated from 13 February to 13 March 2013, encompassing the anticyclone passage.

2.1. Lead Fraction Definition

neXtSIM uses three ice categories; *new ice* (frazil ice formed in open water), *young ice* ($\lesssim$25 cm), and *old ice* ($\gtrsim$25 cm) and thus explicitly represents the thin and newly formed ice in leads (Rampal et al., 2019). When leads form in winter they quickly refreeze and become a mixture of open water and thin ice (Beitsch et al., 2014). Based on this, we define a lead fraction as the combined fraction of open water and young ice. A grid cell is then considered a lead when the lead fraction exceeds 5%, thereby excluding the thicker pack ice. This approach is comparable to previous lead detection algorithms (e.g., Röhrs & Kaleschke, 2012; Ólason, Rampal, & Dansereau, 2021).

To evaluate the accuracy of the model in capturing the breakup, we compare our results to satellite observations of leads (Arcleads derived from the Moderate Resolution Imaging Spectroradiometer; Willmes & Heinemann, 2015), ice drift from the Ocean and Sea Ice Satellite Application Facility (OSISAF; Lavergne et al., 2010), and sea ice deformation from RADARSAT data (Figure S1 in Supporting Information S1).

3. Simulating the 2013 Sea Ice Breakup Event

Satellite observations show that a fracture was already present by mid-February at Point Barrow in the western Beaufort Sea within an area covered by FYI (Figure 1b). Over the next few days, large pieces of sea ice started to break off and were transported toward the Chukchi Sea. On 23 February, an extensive arch-shaped fracture

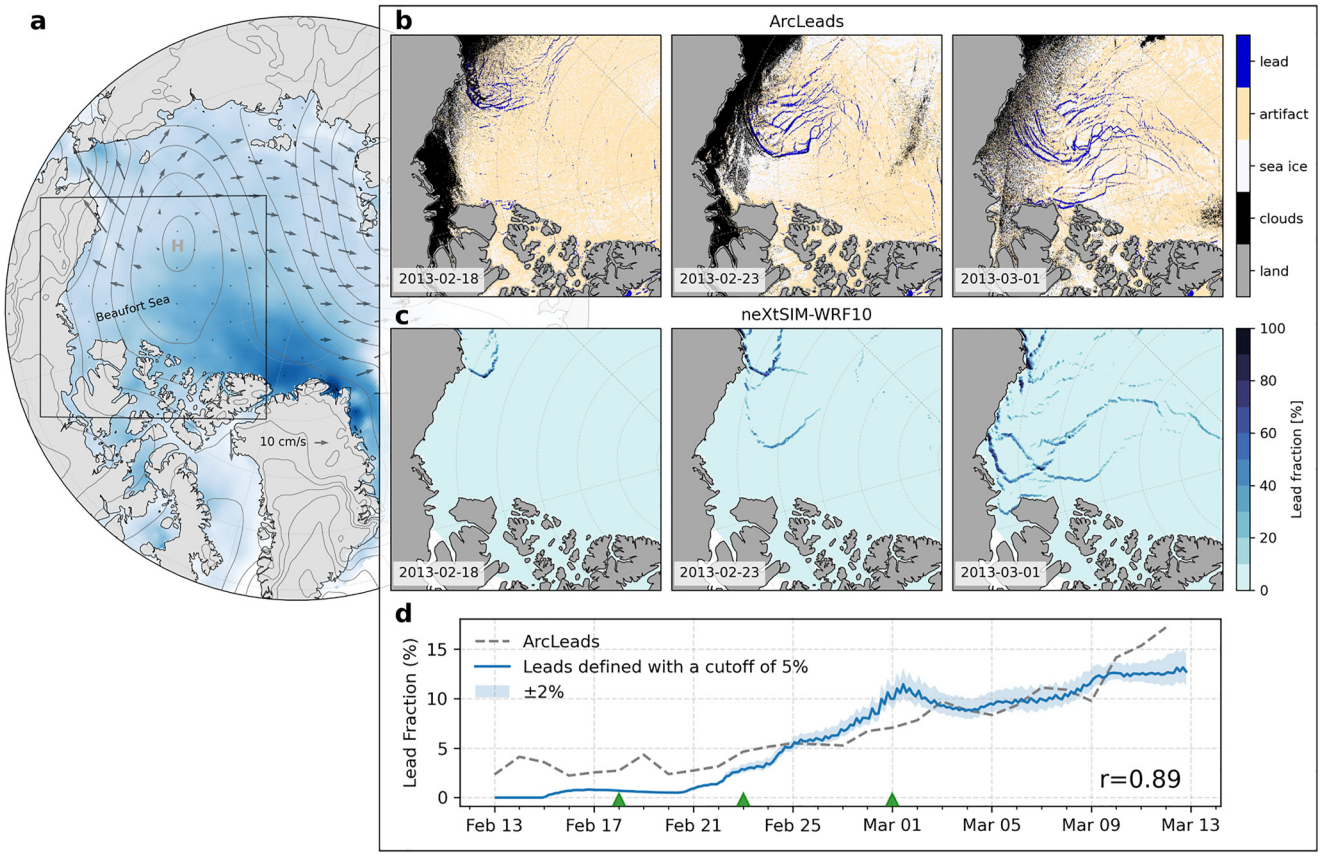

Figure 1. (a) Schematic map of the Beaufort Sea with the observed winter sea ice thickness from CS2/SMOS (shading), ice flow from neXtSIM (arrows), and mean sea-level pressure from ERA5 (solid and gray lines) all shown on 23 February 2013. (b) Daily categorical lead map following Willmes and Heinemann (2015) based on the Moderate Resolution Imaging Spectroradiometer imagery. (c) Simulated lead fraction using WRF10 as the atmospheric forcing. (d) Time series of lead area fraction in the Beaufort Sea for the model (blue) and Arcleads (gray-dashed line). Leads are defined as areas where the lead fraction exceeds 5%. The shading shows the sensitivity to using a threshold value of 3% and 7%, respectively. The r-value is the correlation coefficient between the observed and modeled lead fraction. Both (b and c) for 18, 23 February and 1 March 2013 are marked by green triangles in (d).

about 1,000 km long and ~4 km wide had formed, extending across nearly the entire Beaufort Sea with secondary fractures on the leeward side. By the end of February, the fracturing had expanded toward Banks Island in the east, at which point the ice cover was broken up and consisted of a myriad of free-drifting ice floes. The model shows remarkably good agreement with the observations, both in terms of the spatial pattern (Figure 1c) and the evolution of the lead area fraction in the Beaufort Sea (Figure 1d). In particular, the model captures the characteristic arch-shaped wave of fractures with the first opening close to Point Barrow in mid-February, propagating east toward Banks Island (see also Supporting Information Movie 1).

The simulated breakup pattern is due to a combination of the wind forcing (controlled by the location and strength of the anticyclone) and the coastal geometry. This makes the quality of the atmospheric forcing very important for simulating the breakup. By examining the internal stress state of the sea ice (not shown), we find that the fractures form due to a combination of high shear and comparatively low normal stresses. This is associated with westward winds blowing nearly parallel to the Alaskan coast (Figure 2a), causing sea ice to break tangentially to the coast (as also seen by Lewis & Hutchings, 2019). Once the wind speed exceeds a critical value (about 10 m s^{-1}), the ice breaks and fractures spread eastward in a step-like manner matching the timing of the anticyclone passage (Figure 2b). This critical threshold likely depends on multiple factors, including ice thickness and concentration, wind direction, and sea ice floe size distribution (Rampal et al., 2009; Stern et al., 2018). Overall, the simulated sea ice drift associated with the breakup is remarkably close to the observed drift from OSISAF (Figure 2c), especially in the pack ice (RMSE = 4.9 cm s^{-1}).

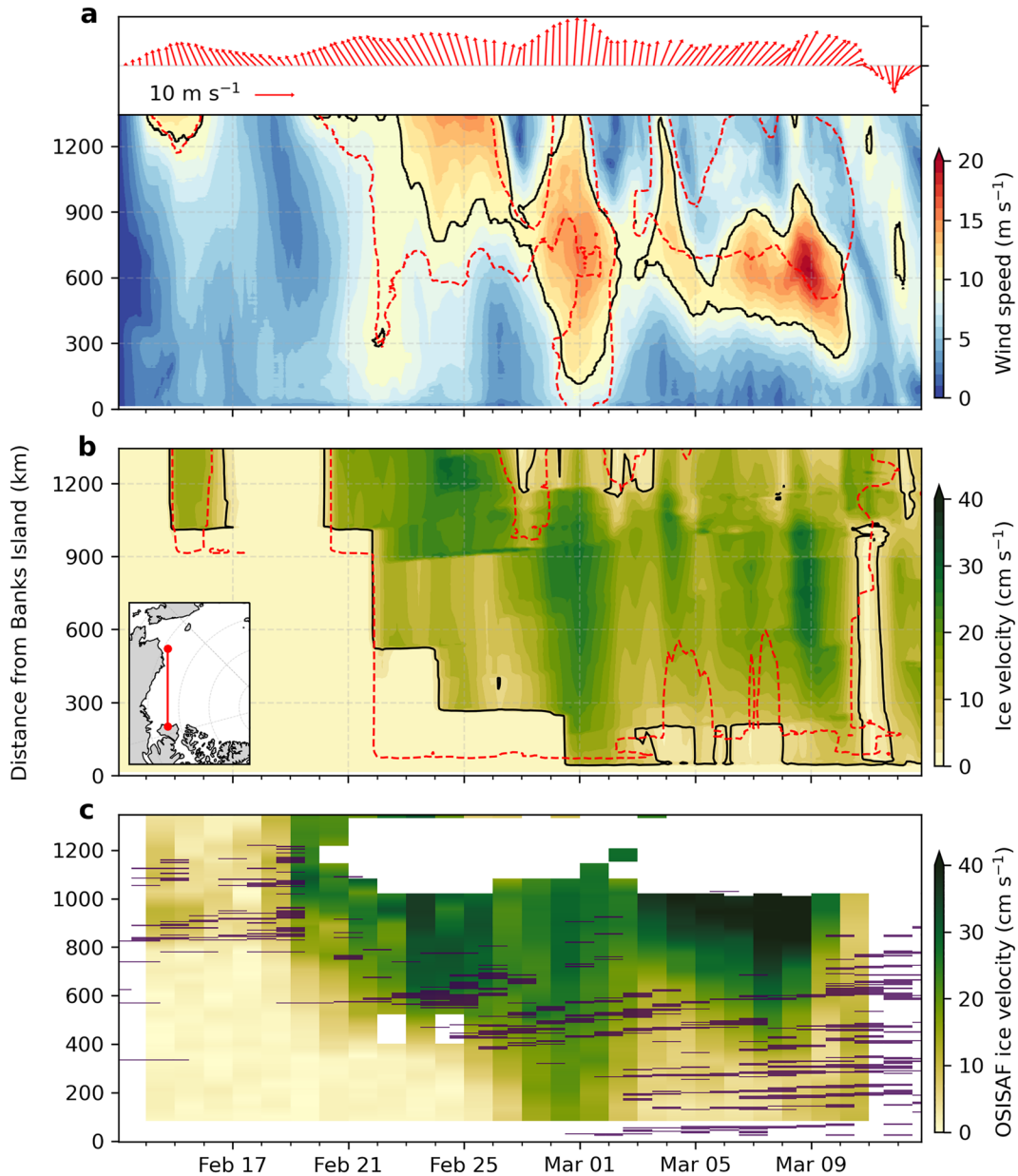

Figure 2. Time series during the breakup event of (a) wind speed and direction (red arrows; up = away from Banks Island), (b) sea ice velocity and lead propagation indicated by the 5-cm s^{-1} ice velocity contour, and (c) observed ice velocity from OSISAF and lead propagation from Arcleads data (purple lines). All variables are calculated along the transect indicated in (b) running from the western Beaufort Sea (close to Point Barrow) to Banks Island. Black lines in (a and b) represent the 10-m s^{-1} wind speed and 5-cm s^{-1} ice velocity, respectively. The red-dashed line corresponds to the WRF80 experiment.

Another important factor for the fidelity of the simulated breakup is the new BBM rheology (Ólason, Boutin, et al., 2021) employed in neXtSIM. Fracturing and threshold mechanics seen in both observations and the simulation are characteristics of the brittle nature of sea ice mechanics (Rampal et al., 2019; Schulson, 2009). In comparison, this is not adequately resolved in traditional elastic-viscous-plastic (EVP) models that typically require a horizontal resolution of about 1 km—between one and two orders of magnitude higher than what is used in the latest CMIP6 climate models—to represent sea ice deformation features at smaller scales (Hutter et al., 2019, 2022; Spreen et al., 2017; Wang et al., 2016). This can be seen from the neXtSIM simulation performed using the modified EVP rheology (mEVP; Figure S1 in Supporting Information S1). Compared to BBM, the mEVP simulates a much smoother sea ice deformation field and does not capture the fracture

propagation (although it does capture some arching at Point Barrow). We expect very high resolution (EVP) models to perform substantially better than the mEVP results shown here, but such experiments are costly and were not attempted here. The role of resolution in reproducing small-scale features in (E)VP models is being actively investigated in the community as well as that of modifying parameters and parameterizations within sea ice models (e.g., J. Zhang, 2021; Bouchat et al., 2022; Hutter et al., 2022).

3.1. Impact of Atmospheric Resolution on Sea Ice Breakup

Regional atmospheric properties, such as weather dynamics and horizontal gradients, are generally more skillfully reproduced at a higher resolution (Lindsay et al., 2014). To test how the simulated breakup is affected by the resolution of the atmospheric forcing, we performed additional experiments with different resolutions of the Polar-WRF model (Figure S2 and S3 in Supporting Information S1). Doing this, we find that using high-resolution forcing (WRF10 or WRF20) yields the characteristic progressive wave of fractures toward Banks Island, which matches the timing of the observed sequence of lead openings quite well (Figures 2b and 2c). Whereas the ice immediately breaks much further east, closer to Banks Island when using the low-resolution forcing.

The improved breakup pattern seen in WRF10 is due to the fact that the location of the anticyclone and associated winds is better reproduced at a higher resolution. In comparison, the lower resolution forcing (WRF40 and WRF80) exhibits stronger winds, exceeding 10 m s^{-1} in the central Beaufort due to an offset in the anticyclone track, causing the ice to break up prematurely (Figure S3 in Supporting Information S1). Hence, despite these relatively modest differences in the location and strength of the anticyclone between the high- and low-resolution forcing, we obtain major differences in the simulated breakup pattern. This underlines the nonlinear, threshold-like response of the ice to the atmospheric forcing.

The difference in the simulated wind fields is, however, not purely due to the resolution itself, but is also related to how the atmospheric dynamics behave at these higher resolutions. We demonstrate this by using the global ERA5 reanalysis, which despite its relatively high resolution of 31 km performed similarly to WRF80 (Figure S2 and S3 in Supporting Information S1). This suggests that not only the resolution but also proper tuning of the atmospheric model (e.g., improved parameterizations optimized for polar regions) is an important factor for simulating sea ice deformation (Hines et al., 2015).

4. Thinning Sea Ice Accelerates Wind-Induced Breakup

Following the minimum extent in 2012, the Beaufort Sea ice cover was exceptionally thin and weak in winter 2013 (Parkinson & Comiso, 2013), which may have preconditioned the breakup. Long-term sea ice thinning could therefore be expected to weaken the sea ice cover further and increase deformation rates (Rampal et al., 2009). To test this, we ran three sensitivity experiments with the initial sea ice thickness (SIT) set at 50% (0.5 × SIT), 150% (1.5 × SIT), and 200% (2.0 × SIT) of that of the control experiment (Figure S4 in Supporting Information S1). The average thickness in the Beaufort Sea for these three scenarios is 0.69 m, 2.01 m, and 2.75 m, respectively (compared to 1.37 m in the control experiment). Thus, for 0.5 × SIT, the winter ice cover mostly consists of thin FYI, which is projected to occur before the end of 2100 by CMIP6 models (Figure S4 in Supporting Information S1). The remaining two cases reflect sea ice conditions prior to the 2000s, when the Beaufort Sea ice cover was considerably thicker (Rothrock et al., 2008).

When the sea ice is thinner, it breaks up more easily and becomes more mobile, while for thicker sea ice, the threshold for initiating breakup is higher. This is because thicker sea ice has a higher mechanical strength compared to thin ice, limiting its fragmentation (Rampal et al., 2009). This relationship between thickness and mobility is reflected in the ratio between sea ice drift and wind speeds (Figure 3a), which increases with thinner ice (e.g., Maeda et al., 2020). In neXtSIM, the mechanical strength is a combination of Coulomb shear failure and a resistance to ridging proportional to ice thickness to the power 3/2 following Hopkins (1998). As a result, the modeled ice cover is more damaged when the sea ice is thin (SIT × 0.5) with more leads (lead fraction increases by ∼3%; Figure 3b), while for thicker ice (SIT × 1.5 and SIT × 2.0), stronger winds (>14 m s^{-1}) are required to break the ice and there is a large reduction in the drift speed. The start of the breakup also occurs progressively later with increasing thickness (21 February for 1.5 × SIT and around 1 March for 2.0 × SIT, Figure 3b), a direct consequence and illustration of thicker sea ice being more resistant to breakups. We caution, however, that the

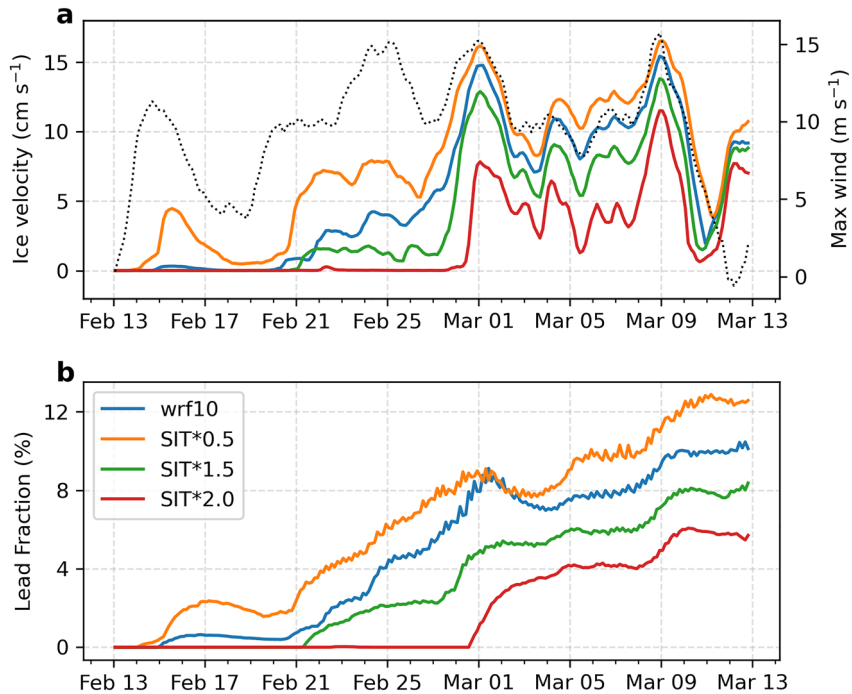

Figure 3. Time series of (a) mean sea ice velocities in the Beaufort Sea and maximum winds (gray-dashed line) in the along-transect direction (inset in Figure 2b). (b) Average lead fraction shown as a % of the total Beaufort Sea area. The area is outlined in Figure 4a.

sensitivity of the simulated failure to changes in ice thickness is likely to be more complicated in reality as the model may not fully reflect the true relationship between ice strength and ice thickness.

5. Local Impact on Ice Thickness and Volume

Opening of leads exposes the relatively warm ocean to the cold atmosphere, resulting in stronger heat and moisture transfers from the ocean to the atmosphere. Locally, heat fluxes in excess of 300 W m^{-2} are found in open leads (Figure S5 in Supporting Information S1), similar to those found in observations (Andreas & Cash, 1999). The enhanced ocean heat loss promotes new ice growth within the leads, which can be seen in the thickness distribution between 0 and 1 m (Figure 4a). During the breakup, the median thickness increases from 1.29 to 1.45 m (16 cm), corresponding to a net increase of 111 km^3 in ice volume (Table S2 in Supporting Information S1). Overall, this is comparable to earlier estimates from Babb et al. (2019) and thickness observations by Richter-Menge and Farrell (2013) obtained during winter 2013.

Changes in ice volume occur due to ice growth (thermodynamics) and ice advection (dynamics). First, we consider the thermodynamic impact of the breakup by estimating the ice growth in the Beaufort Sea for the leads and pack ice separately (see "Methods"). The total thermodynamic ice growth from 13 February to 13 March is 344 km^3 (Figure 4b) and is dominated by sea ice growth in the pack ice (80%). Thus, the formation of new ice in leads yields a ~20% increase (67 km^3) in the Beaufort ice volume. This gives an average growth rate of ~20 cm day^{-1} within leads (Figure S6 in Supporting Information S1), which is similar to growth rates observed in open water during winter (e.g., Skogseth et al., 2009).

The impact of changes in ice dynamics on the sea ice mass budget is illustrated in Figure 4d. As the ice cover becomes more fractured and mobile, more ice is also advected through the Beaufort Sea as a consequence of the strong (westward) winds and enhanced drift speeds (Figure 3a). During the event, there is a net sea ice export of 233 km^3, implying that 2/3 of the ice formed by thermodynamic processes is transported out of the region. Note that as the model underestimates the free ice drift (Figure 2c), the simulated export is likely a conservative estimate. This indicates that extreme winter breakup events may result in a thinner and thus weaker sea ice cover compared to years without any breakups. This can be illustrated by turning off the ice dynamics in the model,

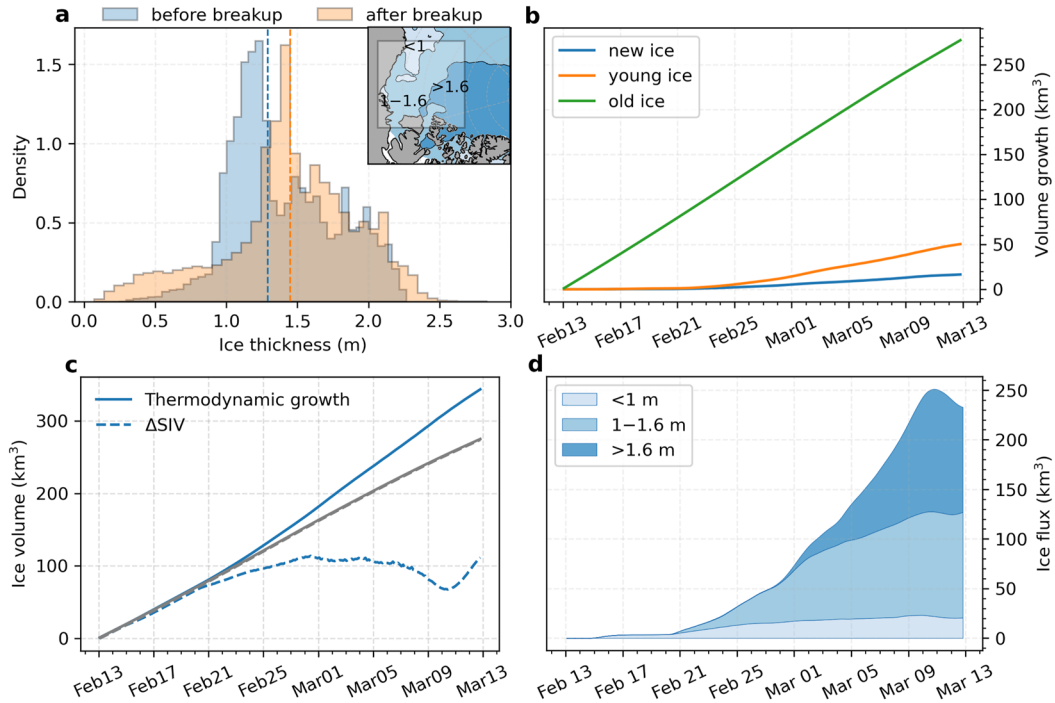

Figure 4. (a) Histograms of the normalized sea ice thickness in the Beaufort Sea before (blue) and after (orange) the breakup event. (b) Cumulative thermodynamic ice growth in the Beaufort Sea, calculated for new ice (blue line), young ice (orange line), and old ice (green line). (c) Total thermodynamic ice growth (solid line) and ice volume change (ΔSIV; dashed line) in the Beaufort Sea for WRF10 (blue) and no_motion (gray). In no_motion, the sea ice dynamics are turned off. (d) Time series of sea ice volume flux, where positive values correspond to an export out of the Beaufort Sea. The total flux is split into contributions from newly formed sea ice (SIT < 1 m), first-year ice (1 > SIT < 1.6 m), and multiyear ice (SIT > 1.6 m). The spatial distribution of the thickness classes is shown in (a) for February 13.

thereby preventing the breakup from occurring (no_motion in Figure 4c). In this case, due to the reduced ice export, there is much larger increase in ice volume (ΔSIV = 277 km^3), which is purely from the thermodynamic growth of pack ice.

During the initial stage of the breakup, it is predominantly FYI (<1.6 m thick) located in the central and southwestern Beaufort that is being exported westward into the Chukchi Sea (see inset in Figure 4a). When the fractures reach Banks Island on 1 March, the thicker and older ice (>1.6 m) is mobilized and subsequently transported to the Canadian Basin. This pattern is largely consistent with the climatological mean sea ice drift in the Beaufort Sea, following the anticyclonic motion of the Beaufort Gyre (Howell et al., 2016). Toward the end of the breakup, the sea ice flux decreases due to a reversal of the wind direction to the southeast (Figure 2a), enhancing transport of MYI located north of Greenland into the Beaufort Sea, where it replenishes the dynamic sea ice loss. Similarly, airborne observations from late March 2013 show a larger amount of MYI in the north central Beaufort Sea and the central Canada Basin compared to the previous year (Richter-Menge & Farrell, 2013).

6. Discussion and Conclusions

6.1. Challenges Simulating Extreme Breakup Events

In this study, we were able to successfully capture the main features of the 2013 breakup and show that it has a significant impact on the evolution of ice volume in the Beaufort Sea during winter. When it comes to the long-term and wider impacts of the breakup, there are some notable limitations of the current study, in part due to the lack of atmospheric and oceanic feedbacks in the model. Opening of leads has considerable influence on the overlying atmosphere (Lüpkes et al., 2008), which in turn has potential implications for the wider Arctic (Mioduszewski et al., 2018). For example, oceanic heat loss within leads causes near-surface temperature to increase by more than 20°C, which could enhance turbulent convection in the atmospheric boundary layer,

driving further breakup and sea ice production. The resulting changes in surface roughness, for example, from enhanced ridging or reduced concentration, could amplify this effect, but is not properly captured when using a constant and uniform atmospheric drag coefficient (Martin et al., 2016). On the other hand, low-level clouds that further increase downward long-wave radiation are often found over leads (Beitsch et al., 2014; Graham et al., 2019), thereby reducing surface heat loss and inhibiting thermodynamic ice growth.

At the ice-ocean interface, the opening of leads can trigger eddy generation through increased buoyancy fluxes that in turn affect large-scale sea ice dynamics and drift (Cohanim et al., 2021). The increase in drift speeds promotes a significant increase in ocean mixing and drives enhanced bottom melt by mixing up warmer water from below (J. Zhang et al., 2013; Graham et al., 2019). Most of these processes and feedbacks occur on small spatial and temporal scales, which are currently beyond the capabilities of CMIP-style models (Hutter et al., 2022), thus highlighting the need for developing sub-grid-scale parameterizations to account for such processes in future climate simulations.

6.2. Potential Implications for Arctic Sea Ice Loss

Although we cannot directly assess the long-term impact from a single modeled event, our findings suggest that sea ice breakup in winter could lead to an overall reduction in Arctic sea ice in the long term. This is supported by Graham et al. (2019) who show that Arctic winter storms may precondition the sea ice cover for a faster summer melt by promoting enhanced lateral melt rates in deformed sea ice. Similarly, Babb et al. (2019) showed that enhanced sea ice export from the Beaufort Sea in winter results in a thinner and weaker ice cover by the start of the melting season, which could promote an earlier breakup of sea ice in spring. This would accelerate the ice-albedo feedback and a further loss of Arctic sea ice (Dai et al., 2019). However, despite the breakup in winter 2013, the Arctic sea ice volume actually increased that year (Tilling et al., 2015), implying that other factors are also important for controlling year-to-year variations in the Arctic sea ice mass budget (e.g., Screen et al., 2011).

As sea ice in the Beaufort Sea continues to thin (Kwok, 2018), our model results suggest that it becomes more vulnerable to wind-driven breakup during winter months. This could affect ice motion further upstream and potentially increase advection of MYI across the Beaufort Sea (Hutchings & Rigor, 2012; Richter-Menge & Farrell, 2013). Here, it becomes more exposed to summer melt (Babb et al., 2019; Kwok & Cunningham, 2010), thereby reducing the survivability of the remaining MYI in the Arctic. If the frequency of extreme weather events (particularly extreme anticyclones) also increases in the future (Walsh et al., 2020), this could lead to more breakup and further amplify the loss of MYI. Ultimately, these findings highlight that winter breakup events may lead to a faster reduction in Arctic sea ice volume than currently projected by coupled climate models (Davy & Outten, 2020).

Acknowledgments
This work was supported by the Bjerknes Centre for Climate Research through the AOI project, the European Space Agency (Grant Nos. AO/1-9595/18/NL/LF and contract no. 4000132195/20/I-NB—"Digital Twin Earth Precursors—Oceans"; contract no. 4000127401/19/NL/LF—"ARKTALAS Hoavva"), and the Research Council of Norway ("ARIA", Grant No. 302934). The model simulations were performed on resources provided by UNINETT Sigma2—the National Infrastructure for High Performance Computing and Data Storage in Norway. The authors thank A. Komarov from Environment and Climate Change Canada for help with accessing Radarsat-2 data and S. Willmes for providing the Arcleads data set. Finally, we wish to thank J. Hutchings and D. Ringeisen for reviewing the manuscript and inspiring discussions that greatly helped improve the paper.

Data Availability Statement

The neXtSIM model output is available at https://zenodo.org/record/5639492#.YYJJLZso9M8. Scripts for data analysis and plotting can be found at https://zenodo.org/record/6607546#.YpjbcTlBxM8 with the https://doi.org/10.5281/zenodo.6607546. The ERA-5 data (Hersbach et al., 2020) were downloaded from the Copernicus Climate Change Service Climate Data Store (C3S) https://cds.climate.copernicus.eu/cdsapp#!/dataset/reanalysis-era5-single-levels?tab=overview. The Arcleads data set (Willmes & Heinemann, 2015) was obtained from https://meteo.uni-trier.de/v2/arcleads.php. The OSISAF data are freely available at MET-Norway (https://osisaf-hl.met.no/).

References

Andreas, E. L., & Cash, B. A. (1999). Convective heat transfer over wintertime leads and polynyas. *Journal of Geophysical Research*, *104*(C11), 25721–25734. https://doi.org/10.1029/1999jc900241

Babb, D. G., Landy, J. C., Barber, D. G., & Galley, R. J. (2019). Winter sea ice export from the Beaufort Sea as a preconditioning mechanism for enhanced summer melt: A case study of 2016. *Journal of Geophysical Research: Oceans*, *124*(9), 6575–6600. https://doi.org/10.1029/2019jc015053

Beitsch, A., Kaleschke, L., & Kern, S. (2014). Investigating high-resolution AMSR2 sea ice concentrations during the February 2013 fracture event in the Beaufort Sea. *Remote Sensing*, *6*(5), 3841–3856. https://doi.org/10.3390/rs6053841

Bouchat, A., Hutter, N., Chanut, J., Dupont, F., Dukhovskoy, D., Garric, G., et al. (2022). Sea ice rheology experiment (SIREx), part I: Scaling and statistical properties of sea-ice deformation fields. *Journal of Geophysical Research: Oceans*, *127*(4). https://doi.org/10.1029/2021jc017667

Bouillon, S., & Rampal, P. (2015). Presentation of the dynamical core of neXtSIM, a new sea ice model. *Ocean Modelling*, *91*, 23–37. https://doi.org/10.1016/j.ocemod.2015.04.005

Cohanim, K., Zhao, K. X., & Stewart, A. L. (2021). Dynamics of eddies generated by sea ice leads. *Journal of Physical Oceanography*, *51*(10), 3071–3092. https://doi.org/10.1175/JPO-D-20-0169.1

Dai, A., Luo, D., Song, M., & Liu, J. (2019). Arctic amplification is caused by sea-ice loss under increasing CO 2. *Nature Communications*, *10*(1), 1–13. https://doi.org/10.1038/s41467-018-07954-9

Dansereau, V., Weiss, J., Saramito, P., & Lattes, P. (2016). A Maxwell elasto-brittle rheology for sea ice modelling. *The Cryosphere*, *10*(3), 1339–1359. https://doi.org/10.5194/tc-10-1339-2016

Davy, R., & Outten, S. (2020). The arctic surface climate in CMIP6: Status and developments since CMIP5. *Journal of Climate*, *33*(18), 8047–8068. https://doi.org/10.1175/JCLI-D-19-0990.1

Forbes, B. C., Kumpula, T., Meschtyb, N., Laptander, R., MacIas-Fauria, M., Zetterberg, P., et al. (2016). Sea ice, rain-on-snow and tundra reindeer nomadism in Arctic Russia. *Biology Letters*, *12*(11), 20160466. https://doi.org/10.1098/rsbl.2016.0466

Girard, L., Bouillon, S., Weiss, J., Amitrano, D., Fichefet, T., & Legat, V. (2011). A new modeling framework for sea-ice mechanics based on elasto-brittle rheology. *Annals of Glaciology*, *52*(57), 123–132. https://doi.org/10.3189/172756411795931499

Graham, R. M., Itkin, P., Meyer, A., Sundfjord, A., Spreen, G., Smedsrud, L. H., et al. (2019). Winter storms accelerate the demise of sea ice in the Atlantic sector of the Arctic Ocean. *Scientific Reports*, *9*(1), 1–16. https://doi.org/10.1038/s41598-019-45574-5

Hersbach, H., Bell, B., Berrisford, P., Hirahara, S., Horányi, A., Muñoz-Sabater, J., et al. (2020). The ERA5 global reanalysis. *Quarterly Journal of the Royal Meteorological Society*, *146*(730), 1999–2049. https://doi.org/10.1002/qj.3803

Hines, K. M., Bromwich, D. H., Bai, L., Bitz, C. M., Powers, J. G., & Manning, K. W. (2015). Sea ice enhancements to polar WRF. *Monthly Weather Review*, *143*(6), 2363–2385. https://doi.org/10.1175/MWR-D-14-00344.1

Hopkins, M. A. (1998). Four stages of pressure ridging. *Journal of Geophysical Research*, *103*(C10), 21883–21891. https://doi.org/10.1029/98JC01257

Howell, S. E. L., Brady, M., Derksen, C., & Kelly, R. E. J. (2016). Recent changes in sea ice area flux through the Beaufort Sea during the summer. *Journal of Geophysical Research: Oceans*, *121*(4), 2659–2672. https://doi.org/10.1002/2015jc011464

Hutchings, J. K., & Rigor, I. G. (2012). Role of ice dynamics in anomalous ice conditions in the Beaufort Sea during 2006 and 2007. *Journal of Geophysical Research*, *117*(C8), C00E04. https://doi.org/10.1029/2011JC007182

Hutter, N., Bouchat, A., Dupont, F., Dukhovskoy, D., Koldunov, N., Lee, Y., et al. (2022). Sea ice rheology experiment (SIREx), part II: Evaluating linear kinematic features in high-resolution sea-ice simulations. *Journal of Geophysical Research: Oceans*, *127*(4). https://doi.org/10.1029/2021jc017666

Hutter, N., Zampieri, L., & Losch, M. (2019). Leads and ridges in Arctic sea ice from RGPS data and a new tracking algorithm. *The Cryosphere*, *13*(2), 627–645. https://doi.org/10.5194/tc-13-627-2019

Johnson, M., & Eicken, H. (2016). Estimating Arctic sea-ice freeze-up and break-up from the satellite record: A comparison of different approaches in the Chukchi and Beaufort Seas. *Elementa: Science of the Anthropocene*, *2016*(4), 000124. https://doi.org/10.12952/journal.elementa.000124

Kwok, R. (2018). Arctic sea ice thickness, volume, and multiyear ice coverage: Losses and coupled variability (1958-2018). *Institute of Physics Publishing*, *13*(No. 10), 105005. https://doi.org/10.1088/1748-9326/aae3ec

Kwok, R., & Cunningham, G. F. (2010). Contribution of melt in the Beaufort Sea to the decline in Arctic multiyear sea ice coverage: 1993-2009. *Geophysical Research Letters*, *37*(20). https://doi.org/10.1029/2010GL044678

Lavergne, T., Eastwood, S., Teffah, Z., Schyberg, H., & Breivik, L. A. (2010). Sea ice motion from low-resolution satellite sensors: An alternative method and its validation in the Arctic. *Journal of Geophysical Research*, *115*(10), 2009JC005958. https://doi.org/10.1029/2009JC005958

Lewis, B. J., & Hutchings, J. K. (2019). Leads and associated sea ice drift in the beaufort sea in winter. *Journal of Geophysical Research: Oceans*, *124*(5), 3411–3427. https://doi.org/10.1029/2018jc014898

Lindsay, R., Wensnahan, M., Schweiger, A., & Zhang, J. (2014). Evaluation of seven different atmospheric reanalysis products in the arctic. *Journal of Climate*, *27*(7), 2588–2606. https://doi.org/10.1175/JCLI-D-13-00014.1

Lüpkes, C., Vihma, T., Birnbaum, G., & Wacker, U. (2008). Influence of leads in sea ice on the temperature of the atmospheric boundary layer during polar night. *Geophysical Research Letters*, *35*(3), 3805. https://doi.org/10.1029/2007gl032461

Maeda, K., Kimura, N., & Yamaguchi, H. (2020). Temporal and spatial change in the relationship between sea-ice motion and wind in the arctic. *Polar Research*, *39*. https://doi.org/10.33265/polar.v39.3370

Martin, T., Tsamados, M., Schroeder, D., & Feltham, D. L. (2016). The impact of variable sea ice roughness on changes in Arctic Ocean surface stress: A model study. *Journal of Geophysical Research: Oceans*, *121*(3), 1931–1952. https://doi.org/10.1002/2015JC011186

Meier, W. (2017). Losing Arctic sea ice: Observations of the recent decline and the long-term context. In D. Thomas (Ed.), *Sea ice* (Third Edit ed., pp. 290–303). Wiley Blackwell.

Mioduszewski, J., Vavrus, S., & Wang, M. (2018). Diminishing Arctic Sea ice promotes stronger surface winds. *Journal of Climate*, *31*(19), 8101–8119. https://doi.org/10.1175/jcli-d-18-0109.1

Nguyen, A. T., Menemenlis, D., & Kwok, R. (2009). Improved modeling of the Arctic halocline with a subgrid-scale brine rejection parameterization. *Journal of Geophysical Research*, *114*(C11), C11014. https://doi.org/10.1029/2008jc005121

Notz, D., & Stroeve, J. (2016). Observed Arctic sea-ice loss directly follows anthropogenic CO2 emission. *Science*, *354*(6313), 747–750. https://doi.org/10.1126/science.aag2345

Ólason, E., Boutin, G., Korosov, A., Rampal, P., Williams, T., Kimmritz, M., et al. (2021). *A new brittle rheology and numerical framework for large-scale sea-ice models*. JAMES. https://www.essoar.org/doi/10.1002/essoar.10507977.4

Ólason, E., Rampal, P., & Dansereau, V. (2021). On the statistical properties of sea-ice lead fraction and heat fluxes in the arctic. *The Cryosphere*, *15*(2), 1053–1064. https://doi.org/10.5194/tc-15-1053-2021

Parkinson, C. L., & Comiso, J. C. (2013). On the 2012 record low Arctic sea ice cover: Combined impact of preconditioning and an August storm. *Geophysical Research Letters*, *40*(7), 1356–1361. https://doi.org/10.1002/grl.50349

Powers, J. G., Manning, K. W., Bromwich, D. H., Cassano, J. J., & Cayette, A. M. (2012). A decade of Antarctic science support through amps. *Bulletin of the American Meteorological Society*, *93*(11), 1699–1712. https://doi.org/10.1175/bams-d-11-00186.1

Rampal, P., Bouillon, S., Ólason, E., & Morlighem, M. (2016). NeXtSIM: A new Lagrangian sea ice model. *The Cryosphere*, *10*(3), 1055–1073. https://doi.org/10.5194/tc-10-1055-2016

Rampal, P., Dansereau, V., Olason, E., Bouillon, S., Williams, T., Korosov, A., & Samaké, A. (2019). On the multi-fractal scaling properties of sea ice deformation. *The Cryosphere*, *13*(9), 2457–2474. https://doi.org/10.5194/tc-13-2457-2019

Rampal, P., Weiss, J., & Marsan, D. (2009). Positive trend in the mean speed and deformation rate of Arctic sea ice, 1979–2007. *Journal of Geophysical Research*, *114*(C5), C05013. https://doi.org/10.1029/2008jc005066

Richter-Menge, J. A., & Farrell, S. L. (2013). Arctic sea ice conditions in spring 2009–2013 prior to melt. *Geophysical Research Letters*, *40*(22), 5888–5893. https://doi.org/10.1002/2013gl058011

Ricker, R., Hendricks, S., Kaleschke, L., Tian-Kunze, X., King, J., & Haas, C. (2017). A weekly Arctic sea-ice thickness data record from merged CryoSat-2 and SMOS satellite data. *The Cryosphere*, *11*(4), 1607–1623. https://doi.org/10.5194/tc-11-1607-2017

Röhrs, J., & Kaleschke, L. (2012). An algorithm to detect sea ice leads by using AMSR-E passive microwave imagery. *The Cryosphere*, *6*(2), 343–352. https://doi.org/10.5194/TC-6-343-2012

Rothrock, D. A., Percival, D. B., & Wensnahan, M. (2008). The decline in arctic sea-ice thickness: Separating the spatial, annual, and interannual variability in a quarter century of submarine data. *Journal of Geophysical Research*, *113*(C5), C05003. https://doi.org/10.1029/2007jc004252

Samaké, A., Rampal, P., Bouillon, S., & Ólason, E. (2017). Parallel implementation of a Lagrangian-based model on an adaptive mesh in C++: Application to sea-ice. *Journal of Computational Physics*, *350*, 84–96. https://doi.org/10.1016/J.JCP.2017.08.055

Schulson, E. M. (2009). Fracture of ice and other Coulombic materials. In *Mechanics of natural solids* (pp. 177–202). https://doi.org/10.1007/978-3-642-03578-4_8

Screen, J. A., Simmonds, I., & Keay, K. (2011). Dramatic interannual changes of perennial Arctic sea ice linked to abnormal summer storm activity. *Journal of Geophysical Research*, *116*(D15), D15105. https://doi.org/10.1029/2011JD015847

Skogseth, R., Nilsen, F., & Smedsrud, L. H. (2009). Supercooled water in an Arctic polynya: Observations and modeling. *Journal of Glaciology*, *55*(189), 43–52. https://doi.org/10.3189/002214309788608840

Spreen, G., Kwok, R., Menemenlis, D., & Nguyen, A. T. (2017). Sea-ice deformation in a coupled ocean–sea-ice model and in satellite remote sensing data. *The Cryosphere*, *11*(4), 1553–1573. https://doi.org/10.5194/tc-11-1553-2017

Stern, H. L., Schweiger, A. J., Stark, M., Zhang, J., Steele, M., & Hwang, B. (2018). Seasonal evolution of the sea-ice floe size distribution in the Beaufort and Chukchi seas. *Elementa: Science of the Anthropocene*, *6*. https://doi.org/10.1525/ELEMENTA.305

Tilling, R. L., Ridout, A., Shepherd, A., & Wingham, D. J. (2015). Increased Arctic sea ice volume after anomalously low melting in 2013. *Nature Geoscience*, *8*(8), 643–646. https://doi.org/10.1038/ngeo2489

Vihma, T. (2014). Effects of Arctic sea ice decline on weather and climate: A review. *Surveys in Geophysics*, *35*(5), 1175–1214. https://doi.org/10.1007/s10712-014-9284-0

Walsh, J. E., Ballinger, T. J., Euskirchen, E. S., Hanna, E., Mård, J., Overland, J. E., et al. (2020). *Extreme weather and climate events in northern areas: A review* (Vol. 209). Elsevier B.V. https://doi.org/10.1016/j.earscirev.2020.103324

Wang, Q., Danilov, S., Jung, T., Kaleschke, L., & Wernecke, A. (2016). Sea ice leads in the Arctic Ocean: Model assessment, interannual variability and trends. *Geophysical Research Letters*, *43*(13), 7019–7027. https://doi.org/10.1002/2016gl068696

Willmes, S., & Heinemann, G. (2015). Pan-arctic lead detection from MODIS thermal infrared imagery. *Annals of Glaciology*, *56*(69), 29–37. https://doi.org/10.3189/2015AoG69A615

Zhang, J. (2021). Sea ice properties in high-resolution sea ice models. *Journal of Geophysical Research: Oceans*, *126*(1), e2020JC016686. https://doi.org/10.1029/2020JC016686

Zhang, J., Lindsay, R., Schweiger, A., & Rigor, I. (2012). Recent changes in the dynamic properties of declining Arctic sea ice: A model study. *Geophysical Research Letters*, *39*(20), 2012GL053545. https://doi.org/10.1029/2012gl053545

Zhang, J., Lindsay, R., Schweiger, A., Steele, M., Lindsay, R., Schweiger, A., & Steele, M. (2013). The impact of an intense summer cyclone on 2012 Arctic sea ice retreat. *Geophysical Research Letters*, *40*(4), 720–726. https://doi.org/10.1002/grl.50190

Zhang, Y., Cheng, X., Liu, J., & Hui, F. (2018). The potential of sea ice leads as a predictor for summer Arctic sea ice extent. *The Cryosphere*, *12*(12), 3747–3757. https://doi.org/10.5194/tc-12-3747-2018